Electroanalysis, 5(1993) 627-639

REVIEW ARTICLE

Theory of Ultramicroelectrodes

Koichi Aoki
Department of Applied Physics, Faculty of Engineering, Fukui University, 9-1, Bunkyo 3-chome, Fukui-shi 910, Japan
Received October 27, 1992.

ABSTRACT

This review describes the theory of mass transport at ultramicroelectrodes that have broken through several experimental limitations of electrochemical measurements. On the basis of the mathematical miniaturization, the ultramicroelectrode can be classified into a point electrode, a line electrode, and a plane electrode. Electrochemical features of these electrodes are described from a viewpoint of the mass transport, especially due to diffusion. Theoretical difficulty in ultramicroelectrodes is mainly due to nonuniform current distribution on the electrode surface. The expression for the time-dependent diffusion-controlled current at any electrode geometry, which predicts the current responding to any potential variation, is presented. Conditions of the steady-state current are specified. The diffusional characteristic functions at a disk, a cylinder, and a band are presented, from which the theories of various electrochemical techniques can be derived analytically. Voltammetric peak currents at several ultramicroelectrodes are compared in light of the diffusional edge effect. The properties of the steady-state current are described at a disk, a band array, a ring, and a recess electrode. The theory is extended to the current-potential curves complicated by the heterogeneous kinetics at a disk, a cylinder, and a band-array electrode.

KEY WORDS: Ultramicroelectrodes, Theory, Mass transport.

INTRODUCTION

Miniaturization sometimes creates new technological fields, such as the IC technology and micromachines. This is not an exception in the electrochemical field. Miniaturization of electrodes has broken through several experimental limitations of electrochemical measurements [1,2], has provided considerable new information [2,3], and has been useful for exploring new environments. It is now a standard and inevitable tool and plays a significant role [4] in a rapid electrochemical measurement in resistive solution, spatial resolution analysis, a sensor of *in vivo* measurements, and electrode kinetics under the steady-state condition. In order to reveal characteristics of ultramicroelectrodes, it is necessary to realize mass transport at the electrodes. This review describes, in general, the concept and the theory of mass transport at ultramicroelectrodes. Since this review aims at the theoretical comprehension of ultramicroelectrodes, various numerical techniques are not presented here.

Concept and Properties of Ultramicroelectrodes

Although the definition of the ultramicroelectrode is ambiguous, electrodes whose characteristic length is less than 20 μm are often called ultramicroelectrodes. They also involve an electrode with micrometer length in one direction and with millimeter length in another direction, exemplified by a microcylinder electrode. Even one-dimensional miniaturization can exhibit interesting properties of ultramicroelectrodes. Thus, a reasonable definition is that the ultramicroelectrode provides the noble information which cannot be obtained at a conventionally sized electrode when at least one-dimensional size or local geometry of the electrode is made small.

As an electrode is miniaturized, the following phenomena are observed:

1. Mass transport of the electroactive species is varied from the linear diffusion normal to the electrode surface to the two- or three-dimensional diffusion;
2. the current becomes smaller but is not proportional to the electrode area; and
3. the current density increases.

These properties were early been appraised negatively, because (a) the mass transport is complicated, (b) the S/N ratio, in comparison with external noises, is small owing to the small current, (c) kinetic complications are more involved in the current, and (d) there is technical limitation of manufacturing the electrode. These demerits, however, were overcome by the advantages that they may include new data. The advantages, depending on electrode geometry, are summarized as follows:

1040-0397/93/$5.00 + .25

1. a steady-state or quasi-steady state current is obtained even in a quiescent solution;
2. the steady-state current allows us to make chemical and electrochemical kinetic measurements;
3. the current-potential curve with little deformation renders rapid measurements;
4. highly accurate measurements are possible in nonpolar solvents or resistive solution without deliberately adding supporting electrolytes;
5. local concentration profiles and localized analytes can be determined, exemplified by a scanning vibration microscope and a physiological sensor in living tissues; and
6. arrangement of ultramicroelectrodes provides new functionality owing to reactions of electroactive species.

At present, some of these properties have been elucidated in detail by the theory.

Classification of Ultramicroelectrodes

If characteristic length of a ultramicroelectrode is made infinitesimally small, it tends either to a point, a line, or a plane. On the basis of this mathematical miniaturization, ultramicroelectrodes can be classified into a point electrode, a line electrode, and a plane electrode. The classification will be consistent with the electrode behavior through the mass transport mode, as shown in the next section. Although real ultramicroelectrodes are deviated from the three mathematical geometries, the classification is helpful to predict the basic behavior. Table 1 shows characteristics of the three electrodes.

The point electrode looks like a spot with vague geometry at a long distance from the electrode. The concentration profile and potential distribution in the solution are of spherical form. For a long time, they become the steady state and, hence, yields the steady-state current. This current is proportional to the characteristic length (radius) of the electrode. A typical point electrode is a disk electrode inlaid on an insulating plane.

A feature of the line electrode is two-dimensionally concentric distributions of the concentration and the potential. Since the line electrode is of the order of millimeters or centimeters in the direction of the line, the current has similar order to that of the large electrode. Therefore, it is useful for an analytical tool. Indeed, a carbon fiber working as a cylinder electrode has played a vital role in a detector of *in vivo* measurements.

There is a ultrathin ring electrode that shares characteristics of the point electrode and the line electrode. The ring electrode looks like a point from a position very far from the electrode, whereas it looks like a curved line near the electrode. It has the steady-state current because of the feature of the point electrode.

A plane electrode of interest is a microarray electrode, which is composed of point electrodes and line electrodes on a planar insulator. It is versatile in functionality by designing the geometrical arrangement. A mode of mass transport depends basically on whether elementary electrodes are a point or a line electrode.

History of the Theory

A target of the theory of the ultramicroelectrode is to evaluate current or potential responding to electrochemical stimulation. Factors determining the current or the potential are the charge transfer rate, chemical complications, and mass transport, including diffusion, electric migration, and convection. The diffusion problems have been investigated most extensively because they reflect well the geometry of ultramicroelectrodes. Some of them are classical and, hence, can be found in monographs of thermal conduction of heat [5], electrostatics [6], and diffusion of mathematics [7].

The most classical and well-known theory is the steady-state current at a spherical electrode [8]. This is essentially equivalent to a problem of the potential distribution around an isolated conducting sphere [6]. The diffusion problem at the disk electrode, called the Weber problem [9], was solved by Tranter [10], Grigull [11], and Saito [12]. A number of investigations on ultramicroelectrodes have been focused on the disk electrode, partly because it exhibits most strongly properties of ultramicroelectrodes and partly because it can be fabricated closely to the model.

When a potential is applied to the electrode, the responding current decreases to the steady state. Such transient behavior has been predicted theoretically by Aoki and Osteryoung [13]. The transient currents at a short time [14,15] and at a long time [16,17] have been ex-

TABLE 1 Characteristics of the Three Kinds of Electrodes

Electrode	*Point*	*Line*	*Plane*
Concentration profile	Sphere	Cylinder	Plane
Basic diffusion functions	Legendre and Bessel	Bessel	Exponential[a]
Current at a long time	Steady state	Quasi-steady state	Tending to zero[a]
The first two terms of $(a/D)f(t)$	$(\pi\theta)^{-1/2} + 1$[b]	$(\pi\theta)^{-1/2}$ + (from 0.4 to 0.5)	$(\pi\theta)^{-1/2a}$
Examples	disk	cylinder	disk array
	hemisphere	band	band array

[a]At a large planar electrode
[b]$\theta = Dt/a^2$.

amined by some numerical techniques. The theory has been extended into linear sweep voltammetry [18], chronopotentiometry [19], square-wave voltammetry [20], and so on. The disk electrode is influenced by the charge transfer rate owing to the diffusional edge effect, the theory of which will be described in a later section.

The theory of cylinder electrodes has been mostly based on the approach of the heat conduction of cylindrical solids developed by Jaeger and Clarke [21]. Since it covers, however insufficiently, the quasi-steady state at readily available cylinder electrodes, such as carbon fiber electrodes, it has been re-examined in electrochemical applications [22].

The ultramicroband electrode has the possibility of being miniaturized to a few nanometer size if the thin layer technology is applied to the fabrication. Saito derived the expression of the diffusion-controlled current at band electrodes on the assumption of the steady state [12]. It is a loss of physical meaning, however, to make the assumption of the steady state in the two-dimensional space. Oldham derived expressions for a current-time curve at very thin electrodes and applied it to the microband electrode [23]. Aoki et al. derived analytical equations for chronoamperometry [24].

Microarray-disk electrodes have been proposed as a model electrode partially blocked by oxide film or adsorption [25], and some approximate methods of estimating the current have been presented [26,27]. Quantitative analysis of microarray-band electrodes is the steady-state current at an interdigitated microarray electrode [28].

Currents controlled by migration or chemical complications have not been well studied yet because they depend largely on experimental conditions. A systematically, theoretical approach of the current may be pessimistic even in the future.

COMPREHENSIVE THEORY

Mass Transport

Mass transport at ultramicroelectrodes is caused by diffusion, electric migration, and convection of electroactive species, as at large electrodes. Since the convection often suppresses most advantages of ultramicroelectrodes, it is beyond the main subject, except the diffusional edge effect [29] or analytical applications at microband array electrodes in a channel flow [30].

Mass transport by diffusion and migration is brought about by local gradient of electrochemical potential of the electroactive species. Let the concentration of the electroactive species i be c_i, the diffusion coefficient be D_i, the number of charge be z_i and the inner potential in the solution be ψ. Then the transport rate J_i is given by the Nernst-Plank equation [31]

$$\mathbf{J}_i = -D_i \operatorname{grad} c_i - (z_i F/RT) D_i c_i \operatorname{grad} \psi \qquad (1)$$

This is independent of electrode geometry. Substituting Equation 1 into the equation of continuum $\partial c_i/\partial t = -\operatorname{div} \mathbf{J}_i$ yields

$$\frac{\partial c_i}{\partial t} = D_i \Delta c_i + (z_i F/RT) D_i (\operatorname{grad} c_i) \cdot (\operatorname{grad} \psi) + (z_i F/RT) D_i c_i \Delta \psi \qquad (2)$$

where "·" denotes an inner product. This is a basic equation of time-dependent mass transport. Since explicit forms of the Laplacian and the gradients in Equation 2 depend on the geometry of an electrode and its support as well as the arrangement of a reference and a counter electrode, Equation 2 involves geometrical information implicitly through given boundary conditions.

Equation 2 can be classified into three categories, depending on the magnitude of grad ψ.

1. When concentrations of supporting electrolytes are high enough to yield uniform potential distribution (grad $\psi = 0$), Equation 2 is reduced to Fick's second law. Geometrical effects are involved only in Δc_i.
2. When grad ψ varies with concentrations of supporting electrolytes regardless of those of the electroactive species, the Laplace equation ($\Delta\psi = 0$) holds under the boundary conditions of cell and electrode geometry. Then grad ψ in Equation 2 can be evaluated by solving the Laplace equation, being independent of Equation 2.
3. When concentrations of supporting electrolytes are so small that the electric neutrality breaks down in the vicinity of the electrode, the Laplace equation should be replaced by the Poisson equation given by $\Delta\psi = -(1/\epsilon_0\epsilon_s) \sum z_i F c_i$, where ϵ_0 and ϵ_s are, respectively, the permittivity of vacuum and the relative permittivity of solution. The concentrations of electroactive species are determined with both Equation 2 and the Poisson equation. Since the Poisson equation includes z_i, the concentration profile varies with mechanisms of electrode reactions. For example, the concentration profile for $O^+ + 2e^- \rightleftharpoons R^-$ is different from that for $O^{2+} + 2e^- \rightleftharpoons R$. Thus, it is difficult to establish systematic theory of the migration effects [32–34].

Solution of Time-Dependent Diffusion Equation (grad $\psi = 0$)

The time derivative in Equation 2 can be solved by the Laplace transformation with respect to time, regardless of grad ψ. The Laplacian takes different forms varying with coordinates, on which the characteristics of ultramicroelectrodes are reflected. The coordinates are often selected so that the largest time variation of the diffusion layer is expressed by only one dependent variable. For example, the best choice at a sufficiently long cylinder electrode is the cylindrical coordinate consisting of the radial length (r in Figure 1A) and the rotation around the axis (θ' in Figure 1A). Since θ' has no influence on the equiconcentration contour, the current density is uniform over the electrode surface.

For the disk electrode, the diffusion layer at a short time is almost parallel to the electrode surface, except

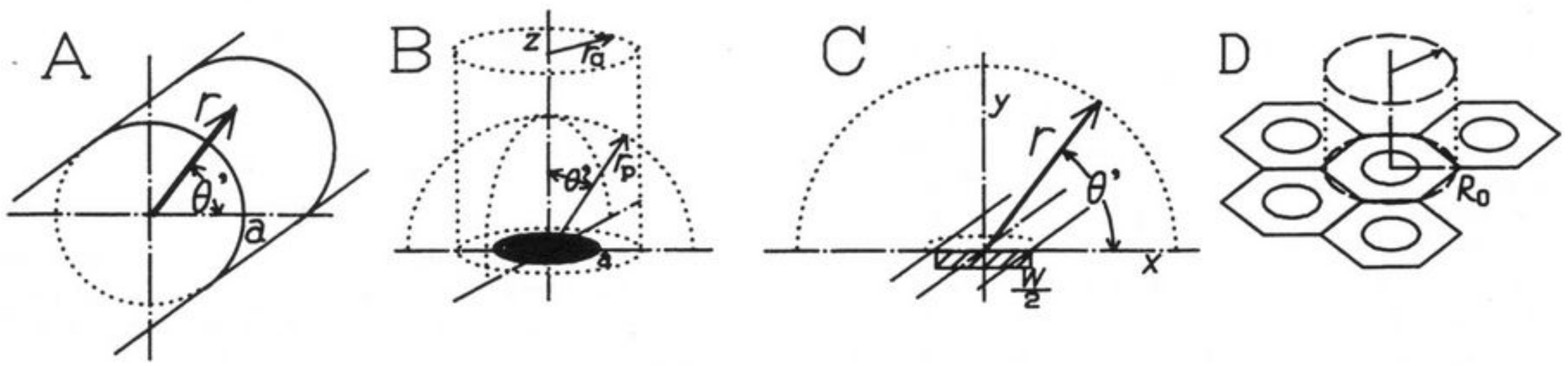

FIGURE 1. Coordinates appropriate to (**A**) a cylinder, (**B**) a disk, (**C**) a band, and (**D**) a disk-array electrode.

the edge, and hence, z (Figure 1B) in the cylindrical coordinate is a predominant variable. The radial length r_c is a secondary variable contributing to the edge effect. Therefore, it is predicted that the edge effect is expressed by an ascending expansion of r_c or the radius. When the diffusion layer grows to a hemicircle in a long time electrolysis, it is represented mainly by the radial distance in the polar coordinate (r_p in Figure 1B) rather than the cylindrical coordinate. A secondary variable θ' in Figure 1B works as location of the electrode on the insulator ($\theta' = \pi/2$). At the microband electrode, the predominant variable in a short time is y in the two-dimensional Cartesian coordinate (Figure 1C). In a long time, y is replaced by r in the two-dimensional cylindrical coordinate.

A functional form is, in general, closely related to a coordinate. When an electrode possesses two coordinates to be best selected, the electrode behavior is expressed by two functional forms depending on the time. For example, the diffusion currents at the disk electrode in a short time and a long time, respectively, are given by the Bessel functions and Legendre functions.

The best choice of the coordinates depends on an expected form of the diffusion layer rather than electrode geometry. This is the case with the numerical calculation of initial-boundary value problems of the mass transport. Formally equispatial discretization in the finite difference method sometimes provides large errors or astronomically long computation time. Intelligent discretization takes unit cells along predicted equiconcentration contours.

Diffusion-Controlled Current Response

In the classical theory of electrochemical techniques developed by Matsuda and Ayabe [35], a solution of the diffusion equation is expressed by the relation between the concentration and the flux at the electrode surface without imposing electrochemical boundary conditions. Therefore, the diffusion problem has been able to discriminate against the electrochemical techniques, such as linear sweep voltammetry and pulse voltammetry. A similar method was applied to hydrodynamic voltammetry at a rotating disk electrode and has extended its applicability. This method is based on the uniform accessibility or uniform current distribution at the electrode. Unfortunately, ultramicroelectrodes rarely provide uniform current distribution owing to the edge effect.

When the charge transfer rate is so rapid that the Nernst equation holds, the concentration at the electrode surface is controlled by the electrode potential and, hence, takes a uniform value. If the average current is used instead of the nonuniform local current density, it may be related to the surface concentration or the electrode potential. For this purpose, the initial-boundary value problem in the three-dimensional diffusion space has been solved [36] for any electrode geometry by means of a technique of the Green function. The total current I is then expressed by the convolution integral of both diffusional response function $f(t)$ and the time-dependent electrode potential $E(t)$, as follows:

$$I = nFAc^* \frac{\mathrm{d}}{\mathrm{d}t} \int_0^t \frac{f(t-u)}{1 + \exp\left[-nF(E(u) - E^{\oplus\prime})/RT\right]} \mathrm{d}u \tag{3}$$

where c^* is the bulk concentration of the electroactive species, A is the geometrical area of the electrode, and $E^{\oplus\prime}$ is the formal potential of the redox reaction. The function $f(t)$ depends on electrode geometry. For a large planar electrode, it is given by $f(t) = \sqrt{D/\pi t}$. According to the theoretical work by Oldham [37], $f(t)$ at any smooth electrode is given by

$$f(t) = \sqrt{D/\pi t} + C + \text{terms of order } t^{1/2}, t, t^{3/2} \tag{4}$$

where C is a constant. Carrying out differentiation of Equation 3 yields

$$I = nFAc^* \left\{ \frac{f(t)}{1 + \exp\left[-nF(E(0) - E^{\oplus\prime})/RT\right]} + \frac{nF}{4RT} \int_0^t \left(\frac{\mathrm{d}E}{\mathrm{d}u}\right) f(u)\,\mathrm{sech}^2\left[\frac{nF}{2RT}(E(t-u) - E^{\oplus\prime})\right] \mathrm{d}u \right\} \tag{5}$$

If a functional form of $f(t)$ is known, the time-dependent current can be evaluated from the integration of Equation 5 for a given potential-controlled electrochemical technique. For the case of a potential step, $\mathrm{d}E/\mathrm{d}t$ in Equation 5 should be treated as a delta function.

Equation 5 indicates that the diffusional characteristics [$f(t)$] are independent of the electrochemical techniques [$E(t)$] for the reversible case. In other words, a subject of the mass transport is segregated from the electrochemical boundary conditions, as is the classical theory. The segregation is, however, limited to the rapid charge transfer process.

Steady-State Current

The steady state for diffusion-controlled mass transport is established when (a) a redox oxidized species is reduced at an electrode and is subsequently oxidized at the adjacent electrode or (b) the diffusion layer is in the form of a sphere or a part of a sphere. In either case, the diffusion equation is reduced to the Laplace equation with respect to c_i.

Case (a) requires that both anode and cathode are within a common diffusion layer. The time of establishing the steady state is of the order of l^2/D, where l is an average distance between the two electrodes. The boundary conditions are complicated by the location of the two electrodes. When the concentration profile is two-dimensional, the Laplace equation is often solved by the use of the theory of complex variables [38]. Especially when the diffusional space is surrounded with polygonal insulators including the infinite boundary, the mapping of the complex variables, called Schwarz-Christofell transformation [39], reduces the cell configuration to a simple cell composed of parallel electrodes with the same size. An interdigitated array electrode with alternately arranged anodes and cathodes is an example of this transformation [28].

The superposition principle of the coulombic force is helpful for estimating concentration profiles. It has been applied to evaluating the capacitance [40] and diffusion-controlled current [41,42] at ultrathin microring electrodes. It is, however, difficult to determine the mirror image of the real electrode geometry, and hence, the geometry is sometimes approximately deformed, exemplified by the scanning electrochemical microscope for detecting local corrosion [43].

There is no steady-state solution of the one- or the two-dimensional diffusion with infinite boundaries [case (b)]. A steady-state current exists only in the spherical diffusion [$\partial^2 c_i/\partial r^2 + (2/r)\partial c_i/\partial r = 0$]. The flux ($I/nF$) of the electroactive species is then balanced with the sum of the fluxes J across a spherical diffusion layer in radius R_d much larger than the electrode length, *i.e.*, $I/nF = 4\pi R_d^2 J$. This is demonstrated as follows: If the equation of continuum under the steady state ($\partial c_i/\partial t = -\text{div}\, J_i = 0$) is expressed by the angle-independent polar coordinate, we have

$$-\frac{1}{r^2}\frac{\partial(r^2 J)}{\partial r} = 0 \tag{6}$$

The solution is obviously $r^2 J = Constant$, and hence, the current is also constant.

The steady-state current at the point electrode is proportional to the one-dimensional length of the electrode, rather than the electrode area. This fact is demonstrated as follows. The flux in the solution is proportional to r^{-2} according to the relation $r^2 J = Constant$. Since the flux is equivalent to grad c_i or since the concentration profile is given by the integral of the flux, the concentration has r^{-1} dependence. From the boundary conditions in the bulk and on the electrode surface, the concentration can be approximately expressed by $c \simeq c^*(1 - r_1/r)$, where r_1 denotes a one-dimensional length of the electrode. The flux at the electrode is then given by

$$D(\partial c/\partial r)_{\text{at the electrode}} = Dc^*/r_1 \tag{7}$$

Since the area of the electrode is of the order of r_1^2, the total current is proportional to Dc^*r_1. This is a survey of the proportionality with the one-dimensional length.

DISK ELECTRODE

Steady-State Current

The diffusion-controlled current I_s under the steady state at the disk electrode in radius a has been evaluated [10–12] by the method of the Bessel expansion and is expressed by

$$I_s = 4nFc^*Da \tag{8}$$

In order to grasp correspondence between Equation (8) and the Cottrell equation, I_s is assumed to be equated with $(\pi a^2)nFc^* \sqrt{D/\pi t}$. The time in the Cottrell equation is then $t = 0.2$ ms for $a = 1$ μm and $D = 10^{-5}$ cm^2 s^{-1}. This is too short to be observed by conventional techniques, and hence, extraordinary high current density is established under the steady state.

Let us compare Equation 8 with the hemispherical electrode with the same radius. Since the steady-state current at the hemispherical electrode is expressed by $2\pi nFc^*Da$, it is 1.57 times larger than the current at the disk electrode. The ratio (twice) of the area is not reflected to the steady-state current, as has been demonstrated in the previous section.

The current density j at any radius r on the disk electrode is given by [9]

$$j = (2/\pi)nFc^*D/\sqrt{(a^2 - r^2)} \tag{9}$$

The current density at the edge is infinite because of sharp bending of the current lines near the edge. The infinite current density is compensated with finite values of the heterogeneous electrode reaction rate in the real system.

Time-Variations of Current

The evaluation of the decay of the current responding to a large potential step was a significant target of the theory of the ultramicroelectrode. Flanagan and Marcoux were first to evaluate the current decay curve by the digital simulation [14]. Aoki and Osteryoung derived analytical equations for the current for a short time and a long time [13] by the Wiener-Hopf technique [44]. Since this approach is too sophisticated to be explained, only

the result is described here. The transient current I is expressed by the series expansion of the dimensionless time $\tau = 4Dt/a^2$ and is give by

$$I = 4nFc^*Da\{1 + 0.71835\tau^{-1/2} + 0.05626\tau^{-3/2} - 0.00646\tau^{-5/2} \ldots\} \quad \text{(for large values of } \tau) \tag{10}$$

$$I = 4nFc^*Da\{(\pi/4\tau)^{-1/2} + \pi/4 + 0.094\tau^{1/2} \ldots\} \quad \text{(for small values of } \tau) \tag{11}$$

These two curves overlap in the domain $0.82 < \tau < 1.44$. Equation 10 is the expansion due to the polar coordinate, whereas Equation 11 is due to the cylindrical coordinate.

A more convenient expression has been obtained empirically by Shoup and Szabo [17] by means of the numerical computation of the boundary value problem. The equation that is modified to be applicable to Equation (5) is

$$f(t) = \frac{D}{a}\left\{\frac{a}{\sqrt{\pi Dt}} + 1 + \left(\frac{4}{\pi} - 1\right) \times \exp[-0.391a^2/Dt]\right\} \tag{12}$$

Since this holds for any value of τ, it can be used for quantitative analysis in various electrochemical techniques.

Figure 2 shows the plot of $(a/D)f(t)$ against $\log (Dt/a^2)$. It also shows variations of the diffusional response functions at a large planar electrode ($\sqrt{D/\pi t}$) and at a hemispherical electrode, given by

$$f(t) = \frac{D}{a}\left(\frac{a}{\sqrt{\pi Dt}} + 1\right) \tag{13}$$

Comparison of these curves indicates that the current density ($f(t)$) at the disk electrode is larger than that at the hemispherical electrode near the steady-state domain and much larger than that of the planar electrode. The difference is due to the diffusional edge effect.

Linear Sweep Voltammetry

Theoretical expressions of linear sweep voltammograms or cyclic voltammograms can be derived from Equations (5) and (12) and the condition of the potential sweep, $E = E_i + vt$, where E_i is the initial potential and v is the sweep rate. Taking the initial potential to be sufficiently negative and introducing the dimensionless potential, defined by

$$\zeta = nF(E - E^{\ominus'})/RT \tag{14}$$

we have the expression for the anodic current [18]

$$I = (4nFc^*Da)\frac{p^2}{16}\int_0^\infty \left\{\frac{1}{\sqrt{\pi x}} + 1 + \left(\frac{4}{\pi} - 1\right) \exp\left[-\frac{0.391}{\sqrt{x}}\right]\right\} \operatorname{sech}^2\left(\frac{\zeta}{2} - \frac{p^2}{8}x\right)dx \tag{15}$$

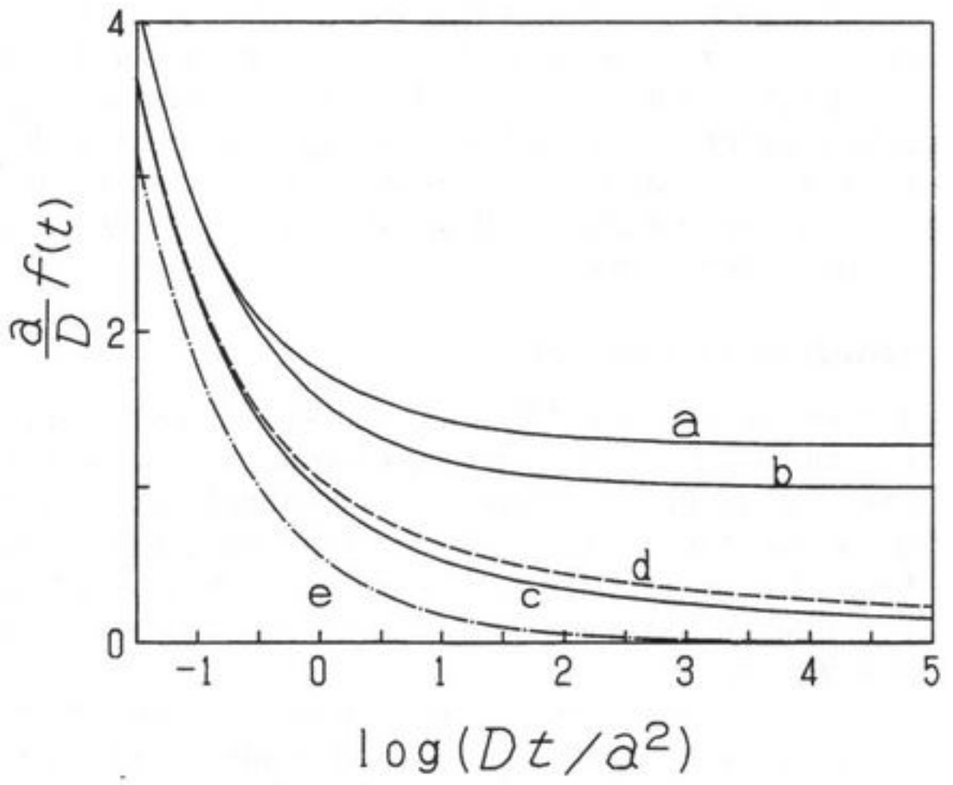

FIGURE 2. Variations of diffusional response functions $(a/D)f(t)$ for (**a**) a disk, (**b**) a hemisphere, (**c**) a cylinder, (**d**) a band, and (**e**) a large planar electrode, where a for the band electrode means $w/2$.

where p is a ratio of the potential sweep rate $(nF/RT)av$ to the diffusion rate D/a, given by

$$p = \sqrt{nFa^2v/RTD} \tag{16}$$

The dimensionless current-potential curve (I/nFc^*Da versus ζ) is a function of only p.

For large values of p or $a\sqrt{v}$, Equation (15) is identical with the equation for linear sweep voltammograms at a large planar electrode [35]. On the contrary, Equation (15) for small values of p or $a\sqrt{v}$ approaches the steady-state solution given by Equation (8).

It is the peak or the maximum current, I_p, that characterizes quantitatively the voltammogram. The peak current has been evaluated numerically from Equation (15) as a function of p and is expressed empirically by [18]

$$I_p = 4nFc^*Da\{0.34e^{-0.66p} + 0.66 - 0.13e^{-11/p} + 0.351p\} \tag{17}$$

Figure 3 shows the plot of the average density of the peak current ($j_p = I_p/(\pi a^2)$) against p. Since the average density for $p > 2$ has approximately linear relation to p, the exponential term in Equation (17) can be negligible. Thus, we have

$$I_p \simeq c^*\{2.64nFDa + 1.4n^{3/2}F^{3/2}a^2\sqrt{D/RT}\} \tag{18}$$

The first term indicates the steady-state solution, except the coefficient, whereas the second is the peak current at a large planar electrode. Therefore, I_p can be expressed conceptually by the sum of the steady-state wave and the conventional voltammogram.

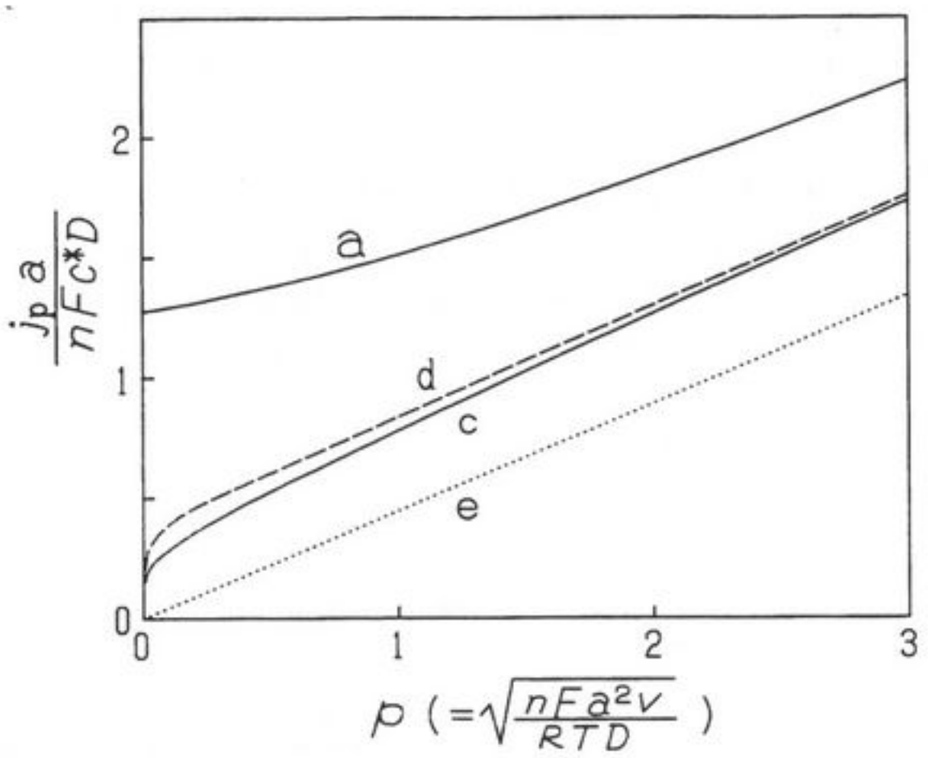

FIGURE 3. Dependence of peak current density, j_p, of linear sweep voltammogram on the dimensionless variable p at (**a**) a disk, (**c**) a cylinder, (**d**) a band, and (**e**) a large planar electrode, where a for the band electrode means $w/2$.

Kinetics of Charge Transfer Reaction under the Steady State

Conventional techniques of fast electrode kinetics are ac impedance and pulse methods with short time responses. Alternatively, the kinetic work under the steady state can be made with hydrodynamics at a rotating disk electrode (RDE) [45]. In either case, a key of the kinetic study is to enhance the current density by the short time measurement or the vigorous convection. Since the steady-state current at a disk electrode 1 μm in diameter is so high that it corresponds to the Cottrell current at 0.2 ms, it may be subjected to the kinetic effect.

According to Equation (9), the current density at the edge is infinite. This is unrealistic, and hence, the current always involves the effect of the charge transfer rate. Discussion on the relation of the infinite current density with the charge transfer rate has also been found in the hydrodynamic voltammetry at the rotating ring electrode [46] and at the channel electrode [47].

The problem of the steady-state diffusion mixed with the charge transfer rate has been first solved analytically by use of the combination of the Mellin transformation and Wiener-Hopf method by Aoki et al. [48]. Bond et al. [49] and Fleischmann et al. [50] derived analytical equations by applying Bessel integrals. Barker and Verbrugge [51] obtained numerical solutions by means of elliptic integrals [52]. Although these four approaches are different in apparent expressions and derivation, they were essentially the same. Oldham and Zoski compared the latter three results [53].

We consider the kinetic equation of the Butler-Volmer type with formal rate constant $k^{\ominus\prime}$, and the cathodic and the anodic transfer coefficients, α and β, respectively. When the diffusion coefficients of the oxidized and the reduced species have a common value and the reduced species is present in the bulk, the current-potential curve is approximated [53] by

$$\frac{I(1 + e^{-\zeta})}{I_s} = \lambda \Big/ \left\{\lambda + \frac{2\lambda + 12}{\lambda + 3\pi}\right\} \tag{19}$$

where

$$\lambda = \frac{k^{\ominus\prime} a}{D}\{e^{-\alpha\zeta} + e^{\beta\zeta}\} \tag{20}$$

This can be applied to simulation of the current-potential curve from known values of the kinetic parameters and the electrode radius.

Of practical significance is the determination of the kinetic parameters from observed current-potential curves. Aoki et al. [48] have proposed a method of a modified log-plot by evaluating empirically the inverse function of the dimensionless current. The log-plot is given by

$$E = E^* - 2.3\frac{RT}{\beta nF}\log\frac{[1 - (I/I_s)(1 + e^{-\zeta})]^{1.11}}{I/I_s} \tag{21}$$

where

$$E^* = E^{\ominus\prime} - 2.3\frac{RT}{\beta nF}\log\frac{\pi a k^{\ominus\prime}}{4D} \tag{22}$$

A value of ζ can be obtained from Equation (14) if $E^{\ominus\prime}$ is a known value. Values of I/I_s are read from the observed curve at given values of E. When they are inserted into the logarithmic term in Equation (21), a plot of log $1.11[1 - (I/I_s)(1 + e^{-\zeta})] - \log I/I_s$ against E becomes a straight line. The slope provides β and the intercept gives E^* or $k^{\ominus\prime}$ through Equation (22). Abe et al. [54] evaluated the kinetic parameters by this method under the steady-state current.

Other Electrochemical Techniques

Square-wave voltammetry of Osteryoung's type, which has a large pulse amplitude and a fast sweep rate on the base potential, is a rapid and highly sensitive analytical tool [55]. When the potential excitation of the square wave is applied to the disk electrode, the decay of the current response competes with the steady-state current. Whelan et al. [20] investigated the competition, theoretically and experimentally, and found that the voltammogram is in a bell shape, regardless of electrode geometry. Under the convenient square-wave conditions (square-wave amplitude $n\Delta E_{sw} = 50$ mV, pulse step $n\Delta E_s = 10$ mV at 25°C), the peak of the difference current ΔI_p is expressed as

$$\Delta I_p = nFc^*a^2\sqrt{\pi D/\tau_{sw}}\,[1.69\sqrt{D\tau_{sw}}/a + 1.06 + 0.25\exp(-1.6\sqrt{D\tau_{sw}}/a)] \tag{23}$$

where τ_{sw} is the square-wave period. It has been proved theoretically that all the dimensionless square-wave vol-

tammogram of the reversible reaction have the identical bell shape whatever geometry the electrode has [36].

Although chronopotentiometry was not in practical use until recently, it is a good example to understand the time variation of the nonuniform current distribution. The current density is uniform immediately after the imposition of the current I. It varies with the time toward the distribution given by Equation (9). Aoki et al. [19] made the theoretical analysis in the chronopotentiometry and expressed the ratio of the transition time at the disk electrode, τ_d, to that at a large electrode τ_{sd} $(= (\sqrt{\pi}/2)\{nF(\pi a^2)c^*\sqrt{D}\}/I)$ as the following equation:

$$\sqrt{\tau_d/\tau_{sd}} = \frac{0.837 - 0.632(I/I_s) + \sqrt{0.400(I/I_s)^2 + 0.206(I/I_s) - 0.565}}{1 - (I/I_s)} \quad (24)$$

where it holds for $I/I_s > 1$. When $1 < I/I_s < 1.1$, the transition time gets very long. As $I/I_s \rightarrow 1$, the transition time cannot be observed, and hence, the potential tends to a steady-state value.

Effects of Electric Migration

A significant advantage of the ultramicrodisk electrode is a possibility of controlling the potential, even in the highly resistive solution, without a loss of accuracy. The solution resistance of 1 MΩ for the current of 10 nA provides only 10 mV of the IR drop. It should be noted, however, that this estimation is only valid for the potential shift but that the migration effect (grad ψ) in Equation 2 is not taken into account. Bond et al. [33] solved approximately the diffusion equation complicated by the migration for a given electrode reaction. Amatore et al. [56] have demonstrated that the migration does not cause large distortion of the voltammogram when the initial charge of the electroactive species is different from the electron number of the charge transfer. Oldham [32] has pointed out from rigorous theoretical analysis that the migration effect is strongly dependent on the charge of the electroactive species. Baker et al. [57] solved the nonlinear ionic transport equation by integral transformation on the assumption that the supporting electrolytes distribute exponentially with respect to the potential. Since a level of the nonlinearity in the mass transport equation varies with the charge of the electroactive species and supporting electrolytes, a systematic approach is so difficult that each experimental system requires each solution of the boundary value problem.

CYLINDER ELECTRODE

Most diffusion problems at the cylinder electrode can be solved rigorously in the same manner as at a large planar electrode if the exponential functions at the planar electrode are replaced by the Bessel functions. The theoretical simplicity of the cylinder electrode is due to concentric equiconcentration contours and the uniform current density at the electrode surface. "A thin electrode" used in this section denotes a cylinder electrode ca. 6–10 μm in diameter, such as a carbon fiber electrode.

Chronoamperometric Curves

By applying Jaeger and Clarke's approach [21] to the diffusion problems at the cylinder electrode in radius a, the diffusion-controlled limiting current j_d is expressed by [58]

$$\frac{j_d a}{nFc^*D} = \frac{2}{\theta^2}\int_0^\infty \frac{\exp[-\theta x^2]}{x\{J_0(x)^2 + Y_0(x)^2\}}dx \quad (25)$$

$$= \begin{cases} \dfrac{1}{\sqrt{\pi\theta}} + \dfrac{1}{2} - \dfrac{\sqrt{\theta}}{4\sqrt{\pi}} + \dfrac{\theta}{8} - 0.147\theta^{3/2} + 0.203\theta^2 + \ldots \text{ for } \theta < 0.18 & (26) \\ \dfrac{2}{\ln(4\theta) - 2\gamma} - \dfrac{2\gamma}{\{\ln(4\theta) - 2\gamma\}^2} + \dfrac{2.624}{\{\ln(4\theta) - 2\gamma\}^3} - \text{ for } \theta > 1200 & (27) \end{cases}$$

where $\theta = Dt/a^2$ and γ $(= 0.57722)$ is Euler's constant. Since Equations (26) and (27) are not a Tayler expansion but an asymptotic expansion, the summation is made up to the term of which the absolute value is minimum. A uniformly convergent expansion valid for any value of θ has not been obtained yet. Two curves for Equations (26) and (27) are not overlapped in the wide domain $0.18 < \theta < 1200$, which includes the domain $2 < \theta < 400$ in the convenient measurement time $(0.05 < t < 10$ s) at the thin electrode. Aoki et al. [22] obtained an empirical equation that was valid for $\theta < 10^6$ by numerical integration of Equation (25):

$$\frac{j_d a}{nFc^*D}\left(= \frac{a}{D}f(t)\right) = \frac{1}{\sqrt{\pi\theta}} + 0.422 - 0.0675\log\theta \pm 0.0058(\log\theta - 1.47)^2 \quad (28)$$

where "±" denotes "+" for $\log\theta > 1.47$ and "−" for $\log\theta < 1.47$.

For a long time electrolysis, the current shows logarithmic dependence of the time. The current observed experimentally at the thin electrode looks like the steady state at $5 < t < 10$. It is thus called the quasi-steady state current. It does not tend to zero within a conventional measurement time. Since $j_d a$ has little dependence on a, the total current is approximately proportional to a.

The variation of $(a/D)f(t)$ in Figure 2 for $Dt/a^2 < 0.1$ is just between curves at the ultramicrodisk electrode and at the planar electrode, indicating that the effect of the lateral diffusion is a half of the point electrode (shown in line 4 of Table 1).

Linear Sweep Voltammetry

Substituting Equation (28) into Equation (5) and using the condition of the potential sweep, the analytical expression of linear sweep voltammogram can be derived [59] as in the linear-sweep voltammetry section. The voltammogram is characterized by p, defined by Equation (16). As values of p decrease, the voltammogram varies from a peaked shape at a large electrode into the

quasi-steady state wave. The peak current density j_p is empirically given by

$$j_p = \frac{n^2F^2c^*av}{RT}\left(\frac{0.446}{p} + \frac{0.335}{p^{1.85}}\right) \quad (29)$$

The plot of the peak current for $p > 0.1$ against v (Figure 2) falls approximately on a straight line. The total peak current at the thin electrode has a linear relation with $a^{1.15}v^{0.075}$, indicating that it is roughly linear with a and is almost independent of v. The behavior is similar to that of the ultramicrodisk electrode rather than that of a planar electrode.

Current-Potential Curves Complicated with Charge Transfer Reactions

Carbon fiber electrodes often change the overpotential with the thermal, the chemical, and the electrochemical treatment. A measure of the overpotential is the difference between the anodic and the cathodic peak potentials of redox voltammograms. A more quantitative appraisal is kinetic parameters of the charge transfer [60].

In order to obtain the kinetic parameters by the use of the cylinder electrode, Aoki et al. [61] presented the analytical expression for the current-potential curves in the normal pulse mode. The current-potential curve for the Butler-Volmer equation has the following two parameters: $\theta = Dt/a^2$ and $(a/D)(\vec{k} + \overleftarrow{k})$ $(= (a/D)\,\vec{k}\,(1 + e^{-\zeta}))$. In addition, the modified log-plot technique has been proposed on the basis of the theoretical curves. The current-potential curves at the thin electrode are approximately subjected to the equation

$$E = E^{\Phi'} + \frac{2.3RT}{\beta nF}\log\frac{k^{\Phi'}a}{0.94D}\frac{(j/j_d)}{\{1 - (j/j_d)(1 + e^{-\zeta})\}^{1.54}} \quad (30)$$

where j_d is the diffusion controlled-current density given by Equation (28) and j is the current density at E. If values of $\log (j/j_d)\{1 - (j/j_d)(1 + e^{-\zeta})\}^{-1.54}$ are plotted against E for known values of $E^{\Phi'}$ and j_d, they fall on a straight line of which the slope and intercept provide, respectively, values of β and $k^{\Phi'}$.

Cyclic voltammetry is more convenient than the pulse techniques because of readily available instruments and partly because of fewer parameters for working. Aoki and Kaneko [62] have explored a technique of estimating the rate constant from the voltammetric peaks. The voltammogram is expressed as a function with the two parameters p $(= \sqrt{nFd^2v/RT})$ and $k^{\Phi'}\sqrt{RT/nFDv}$. For the totally irreversible case at the thin electrode, the anodic peak potential $E_{p,a}$ is given by

$$E_{p,a} = E^{\Phi'} + \frac{RT}{\beta nF}\left[\frac{1.8p\sqrt{\beta}\log(p\sqrt{\beta})}{1.4 + p\sqrt{\beta}} + 1.6 - 2.3\log\frac{k^{\Phi'}a}{D}\right] \quad (31)$$

The potential difference between the anodic peak and the cathodic peak for $\beta = \alpha = 0.5$ is expressed by

$$E_{p,a} - E_{p,c} = \frac{RT}{nF}\left[\frac{7.2p\log(0.71p)}{2.0 + p} + 6.4 - 9.2\log\frac{k^{\Phi'}a}{D}\right] \quad (32)$$

These two equations are convenient for the quantitative appraisal of the activation of carbon fiber electrodes [60].

Other Electrochemical Techniques

All the theoretical approaches developed in the classical polarography can be modified to the cylinder electrode because the flux and the concentration at the electrode are expressed in a closed form. The example is an approach to the catalytic current with the rapid second-order reaction. This has been applied to the evaluation of the second-order reaction rate constant of Fe(edta) with H_2O_2 [63].

Selection of the pulse parameters in pulse voltammetry makes an influence on the diffusion-limiting current if the concentration profile immediately before a given pulse is disturbed by the preceding pulse electrolysis. In the normal pulse mode, the current responding to each pulse is independent of the preceding currents within 5% errors when [pulse width] < [duration between pulse]/10 [64] and is given by Equation (28). On the other hand, the current in the differential pulse mode has minor effects of the preceding pulses because the recorded current is the difference from the base current. The peak current for [pulse width] < [duration between pulse]/3 does not vary with the preceding electrolysis [64]. The peak height is then given by Equation (28) multiplied by $\{\exp(nFE_{pls}/RT) - 1\}/\{\exp(nFE_{pls}/RT) + 1\}$, where E_{pls} is the potential height of the pulse.

BAND ELECTRODE

Characteristic of the band electrode is that the diffusion layer develops from a plane parallel to the electrode surface into a concentric plane centered at the corresponding line electrode. The current density distributes nonuniformly and is especially infinite at the edge of the electrode. This behavior is similar to that of the ultramicrodisk electrode. Because of the nonuniform current distribution and the nonsteady-state current, classical theoretical evaluation of the current has not been presented to our knowledge until attention was paid to ultramicroelectrodes.

Chronoamperometric Curves

The analytical expressions for the current-potential curves were derived by the Wiener-Hopf technique, combined with some integral transformations. The current at a short time, derived by the Fourier transformation, is expressed by [65]

$$I = nFc^*Db\left\{\frac{1}{\sqrt{\pi\theta}} + 1 - \ldots\right\} \quad (33)$$

where $\theta = Dt/w^2$, w is the width of the electrode, and b is the length of the electrode. Equation 33 is valid for $\theta < 2$ within 5% errors. The second term always appears at any electrode with edges [23]. The third term is of the order of $\theta^{3/4}$. The long time behavior has been obtained by the use of the Kontrovich-Levedev transformation to be expressed by [24]

$$I = 2\pi nFc^*Db \int_0^\infty e^{-\theta x} \frac{x^{-1} - 2^{-5} + 2^{-13}x - \ldots}{\{\ln(x/64) + 2\gamma\}^2 + \pi^2} dx$$

$$= 2\pi nFc^*Db\left\{\frac{1}{\ln\theta + 3} - \frac{0.577}{(\ln\theta + 3)^2} - \frac{1.312}{(\ln\theta + 3)^3} - \ldots\right\} \quad (34)$$

It is of interest to compare the behavior at the band electrode with that at the hemicylinder electrode. From Equations (27) and (34), significant terms at the band electrode and the hemicylinder electrode are, respectively, $2\pi/[\ln(Dt/w^2) + 3]$ and $2\pi/[\ln(4Dt/a^2) - 0.6664]$. The correspondence $a \rightarrow w/4$ between the two electrodes proposed by Szabo et al. [66] is valid as rough estimation.

In order to represent the two expansions as a closed form, the empirical equation has been derived: [67]

$$\frac{I}{nFc^*Db} = \frac{w}{D} f(t)$$

$$= \frac{1}{\sqrt{\pi\theta}} + 0.97 - 1.10 \exp\left[-\frac{9.90}{|\ln 12.37\theta|}\right] \quad (35)$$

This is valid for $\theta < 10^8$ and has been verified experimentally [67] and numerically by the polynomial technique [68,69]. The curve of $f(t)$ for $w = 2a$ is shown in Figure 2. Although the variation is similar to that of the cylinder electrode, $f(t)$ for $Dt/a^2 > 1$ is larger by a constant value than that for the cylinder electrode. The enhancement of the current is due to the edge effect.

Chronoamperometry at the band electrode shows better reproducibility than that at the cylinder electrode. This is probably ascribed to a support of the band electrode, which suppresses disturbance of the diffusion layer.

Linear Sweep Voltammetry

When the method described in the linear-sweep voltammetry section is applied to Equations 5 and 35, the expression for the linear sweep voltammetry can readily be obtained [70]. The voltammetric shape is almost the same as that at the cylinder electrode. From the numerical calculation of the voltammograms, the peak current I_p is expressed by

$$I_p = nFc^*Db\left\{0.439p + 0.713p^{0.108} + \frac{0.614p}{1 + 10.9p^2}\right\} \quad (36)$$

where $p = \sqrt{nFw^2v/RTD}$. It is approximately proportional to $v^{0.054}$ at a very thin electrode and at a very slow sweep rate. Comparing the power (0.054) with that of the cylinder electrode (0.075) in Equation 29, the voltammogram at the band electrode is closer to the steady-state current than that at the cylinder electrode, as shown in Figure 3.

In order to estimate the miniaturizing effect at the band and the cylinder electrode, we obtained the relation between w and a at a common value of the peak current. Equating Equation 35 with Equation 29 multiplied by the surface area, extracting a numerically for $v = 50$ mV s^{-1}, $T = 25$°C, and $D = 10^{-5}$ cm^2 s^{-1}, we have $2a/\text{cm} = 0.027\ (w/\text{cm})^{0.72}$, or $w/(2a) = 5.3$ and 2.8, respectively, for $w = 10^{-4}$ cm and 10^{-3} cm. With a decrease in w, the characteristics of the line electrode are manifested more strongly than the cylinder electrode.

DISK-ARRAY ELECTRODE

The disk-array electrode is an assembly of many disk electrodes inlaid on a planar insulator. The current at a short time is just N times of the current at each disk electrode, where N is the number of disks. The growth of the hemispherical diffusion layer causes the overlap with the neighboring diffusion layer. Further overlap makes the diffusion layer a rough plane parallel to the insulator. Then the current looks as if it might come from not only the disks but also the insulator. Thus, a feature of the array electrodes is interplay between the electrodes and the insulator.

In order to make quantitative analysis of the time variation, Gueshi et al. have proposed a model with honeycombed unit cells, each being assumed to be a cylinder [27]. When a disk electrode is on the center of the unit cell R_0 in radius (Figure 1D), the boundary condition $D\partial c/\partial r = 0$ at $r = R_0$ makes each growth of the diffusion layer independent. This type of the diffusion problem, however, has not been solved yet. The difficulty lies in the radial diffusion in the finite domain.

Gueshi et al. solved, approximately, this problem by averaging the radial diffusion [27]. The initial boundary value problem results in formally the classical diffusion problem associated with the first-order preceding reaction. Letting θ_0 be a fraction of the insulator, the chronopotentiometric current I can be related with the transition time τ_{tr} through the following relation:

$$I\sqrt{\tau_{tr}} = \frac{\sqrt{\pi}}{2} nFAc^*\sqrt{D}$$

$$- \frac{\sqrt{\pi\theta_0}}{2\sqrt{l}(1 - \theta_0)} \text{erf}(\sqrt{l\tau_{tr}})I \quad (37)$$

where

$$l = \frac{D}{R_0^2} \frac{2}{\theta_0(1 - \theta_0)\ln\{1 + 0.27(1 - \theta_0)^{-1/2}\}} \quad (38)$$

When I is very large or when the thickness of the diffusion layer is smaller than the disk, it follows that $I\sqrt{\tau_{tr}}/(\sqrt{\pi}/2)nFc^*A\sqrt{D} \rightarrow 1 - \theta_0$. That is, only the geometrical area of the electrode participates in the elec-

trode reaction. Conversely, for a long transition time, Equation 37 becomes

$$I\sqrt{\tau_{tr}} = \frac{\sqrt{\pi}}{2} nFAc^*\sqrt{D} - \frac{\sqrt{\pi}\theta_0}{2\sqrt{l}(1-\theta_0)} I \quad (39)$$

where $I\sqrt{\tau_{tr}}$ is not constant but varies linearly with I.

Expressions for the chronoamperometric curve are more complicated. At a short time electrolysis, the Cottrell current flows corresponding to the geometrical area of the disks. The current for a long time is also Cottrellian with respect to the time, but the magnitude of the current corresponds to the area involving the insulator, as if the insulator might work as an electrode.

This basic approach has been applied to linear sweep voltammetry [71] and the faradic impedance technique [72]. The digital simulation in the present model has provided more accurate results [73,74].

BAND-ARRAY ELECTRODE

The band-array electrode is intriguing in that each band electrode is addressable in potential. Wrighton's group presented a concept of a chemical transistor by modifying the band-array electrode with functional redox polymers [75,76]. Most band-array electrodes have been fabricated by photolithography [75,77].

The interesting, addressing technique is to apply two potentials to every other band electrode alternately. This is called an interdigitated array (IDA) electrode [78]. When one group of the band electrodes is an anode and the other is a cathode, the steady-state current can be observed [79] under the condition that the anodic current is equal to the cathodic one in magnitude. The steady-state current has been well investigated [28] both theoretically and experimentally. The basic theoretical approach is described below.

Since the IDA is regarded as an assembly of the line electrodes, the diffusion occurs in the two-dimensional space. In the repeating unit cell including a half of the anode and a half of the cathode, the two-dimensional Laplace equation holds for the concentration of the electroactive species. Applying the Schwarz-Christoffel transformation to the Laplace equation reduces the cell geometry to the parallel anode and cathode with the same sizes. In the transformed cell, the current density is uniform. Transforming inversely the current density yields the real current I at the IDA in the following form:

$$I = 2mbnFc^*DK(1-q)/K(q) \quad (40)$$

where m is the number of the anode or cathode band electrodes, b is the length of the band, K is the complete elliptic function [80], and q is given by

$$q = \frac{4\sin(\pi w_g/2w_{ge})}{\{1+\sin(\pi w_g/2w_{ge})\}^2} \quad (41)$$

Here, w_g is the gap width between the anode and the cathode, and w_{ge} is the sum of w_g and the common width of the anode or the cathode. Equation 40 is approximated as

$$I = mbnFc^*D\{0.637\ln(2.55w_{ge}/w_g) - 0.19(w_g/w_{ge})^2\} \quad (42)$$

When w_g is larger than a few micrometers, the anodic current is not identical with the cathodic current because of insufficient overlap of the diffusion layer. Thus, a key of establishing the steady state is to make the gap small.

Niwa et al. constructed an IDA-like electrode corresponding to $w_g = 0.5\ \mu m$ by separating the anode and the cathode with a thin film which works as the gap [81]. The steady-state current at this electrode has been numerically evaluated by the boundary element method [82].

The current density under the steady state is enhanced owing to the redox cycle. Thus, it is influenced by the kinetics of the charge transfer rate, of which the current-potential curve has been obtained theoretically [83].

MISCELLANEOUS ELECTRODES

Ring Electrode

The ring electrode is often fabricated as a cross section of an insulating rod on which metal is deposited in a ultrathin film. It is thus a thin ring and has a very long edge, which may provide an intense edge effect.

Since there is a steady-state current at the ring electrode, the boundary value problem results in solving the three-dimensional Laplace equation. A similar problem has already been solved fortunately for the electric capacity of a ring condenser [40,41], and hence, the solution could be directly applied to the diffusion current [42]. The current at the ultrathin ring electrode with a in inner radius and d in outer radius is expressed by

$$I = nFc^*D\frac{\pi^2(a+d)}{\ln 16(d+a)/(d-a)} \quad (43)$$

Since the current varies slightly with the thickness of the ring, it depends almost linearly on the radii rather than the area of the electrode, as is the case for the ultramicrodisk electrode. Owing to the large edge effect, the current distribution is largely nonuniform. The current estimated on the assumption of uniform distribution, nevertheless, agreed well with Equation 43 [84,85], probably because of the ultrathin ring. Transient behavior was predicted analytically [84] and numerically [86].

Recess Electrode

In the recess electrode, an actual electrode is located at the bottom of a hole or a ditch. Since the recess part blocks convection of the electroactive species near the electrode, the current is almost independent of the convection. The recess electrode is a promising detector of flow injection analysis and liquid chromatography. If the convection is vigorous outside of the recess and vanishes within the recess, the steady-state current is essen-

tially the same as that of a thin layer cell. Let L be the depth of the recess. Then the steady-state current is expressed by

$$I = nFc^*AD/L \tag{44}$$

Simple geometry of the electrode is a disk [87] or a band [88]. Theory of linear sweep voltammetry [89] and complication of the charge transfer rate [90] developed in the thin layer cell can be directly applied to the recess electrode.

REFERENCES

1. R. M. Wightman, *Anal. Chem., 53* (1981) 1125A.
2. M. Fleischmann, S. Pons, D. R. Rolison, and P. P. Schmidt, *Ultramicroelectrodes*, Datatech Systems Inc, Morganton, NC, 1987.
3. S. Pons and M. Fleischmann, *Anal. Chem., 59* (1987) 1391A.
4. R. M. Wightman and D. O. Wipf, *Electroanalytical Chemistry*, A. J. Bard, ed., Marcel Dekker, Inc., New York, 1989, vol. 15.
5. H. S. Carslaw and J. C. Jaeger, *Conduction of Heat in Solids*, Oxford University Press, London, 1947.
6. W. K. H. Ponofski and M. Phillips, *Classical Electricity and Magnetism*, Addison-Wesley, Reading, MA, 1969, ch. 5.
7. J. Crank, *The Mathematics of Diffusion*, 2nd ed., Clarendon Press, Oxford, United Kingdom, 1975.
8. A. J. Bard and L. R. Faulkner, *Electrochemical Methods: Fundamentals and Applications*, John Wiley & Sons, New York, 1980, p. 145.
9. J. Crank, *The Mathematics of Diffusion*, 2nd ed., Clarendon Press, Oxford, United Kingdom, 1975, pp. 42–43.
10. C. J. Tranter, *Integral Transforms in Mathematical Physics*, Methuen, London, 1951.
11. I. U. Grigull, *Die Grundgesetze der Warmeuberleitungs*, Spring Verlag, Berlin, 1961.
12. Y. Saito, *Rev. Polarogr. 15* (1968) 177.
13. K. Aoki and J. Osteryoung, *J. Electroanal. Chem. 122* (1981) 19; *160* (1984) 335.
14. J. B. Flanagan and L. Marcoux, *J. Phys. Chem. 122* (1973) 1051.
15. M. Kakihana, H. Ikeuchi, G. P. Satô, and K. Tokuda, *J. Electroanal. Chem. 117* (1981) 201.
16. J. Heinze, *J. Electroanal. Chem. 124* (1981) 73.
17. D. Shoup and A. Szabo, *J. Electroanal. Chem. 140* (1982) 237.
18. K. Aoki, K. Akimoto, K. Tokuda, H. Matsuda, and J. Osteryoung, *J. Electroanal. Chem. 171* (1984) 219.
19. K. Aoki, K. Honda, K. Tokuda, and H. Matsuda, *J. Electroanal. Chem. 182* (1985) 281.
20. D. P. Whelan, J. J. O'Dea, J. Osteryoung, and K. Aoki, *J. Electroanal. Chem. 202* (1986) 23.
21. J. C. Jaeger and M. Clarke, *Proc. Roy. Soc. Edinb. 61A* (1942) 229.
22. K. Aoki, K. Honda, K. Tokuda, and H. Matsuda, *J. Electroanal. Chem. 186* (1985) 79.
23. K. B. Oldham, *J. Electroanal. Chem. 122* (1981) 1.
24. K. Aoki, K. Tokuda, and H. Matsuda, *J. Electroanal. Chem. 225* (1987) 19.
25. K. J. Vetter, *Z. Phys. Chem. (Leipzig) 199* (1952) 300.
26. R. Landsberg and R. Thiele, *Electrochim Acta 11* (1966) 1243.
27. T. Gueshi, K. Tokuda, and H. Matsuda, *J. Electroanal. Chem. 89* (1978) 247, and references there in.
28. K. Aoki, M. Morita, O. Niwa, and H. Tabei, *J. Electroanal. Chem. 256* (1988) 269.
29. K. Aoki, K. Tokuda, and H. Matsuda, *J. Electroanal. Chem. 217* (1987) 33.
30. J. L. Anderson, T. Y. Ou, and S. Moldoveanu, *J. Electroanal. Chem. 196* (1985) 213.
31. A. J. Bard and L. R. Faulkner, *Electrochemical Methods: Fundamentals and Applications*, John Wiley & Sons, New York, 1980, p. 120.
32. K. Oldham, *J. Electroanal. Chem. 250* (1988) 1.
33. A. M. Bond, M. Fleischmann, and J. Robinson, *J. Electroanal. Chem. 172* (1984) 11.
34. C. A. Amatore, B. Fosset, J. Bartelt, M. R. Deakin, and R. M. Wightman, *J. Electroanal. Chem. 256* (1988) 255.
35. H. Matsuda and Y. Ayabe, *Z. Elektrochem. 59* (1955) 494.
36. K. Aoki, K. Tokuda, H. Matsuda, and J. Osteryoung, *J. Electroanal. Chem. 207* (1986) 25.
37. K. B. Oldham, *J. Electroanal. Chem. 297* (1991) 317.
38. E. T. Whittaker and G. N. Watson, *A Course of Modern Analysis*, Cambridge University Press, London, 1973, ch. 5 and 6.
39. R. V. Churchill, J. W. Brown, and R. F. Verhey, *Complex Variables and Applications*, McGraw-Hill Kogakusha, Tokyo, 1974, pp. 239–261.
40. T. J. Higgins and D. K. Reitan, *AIME Trans. 70* (1951) 1.
41. W. R. Smythe, *J. Appl. Phys. 22* (1951) 1459.
42. J. S. Symanski and S. Bruckenstein, *Extended Abstract, 165th Meeting of the Electrochemical Society*, Electrochemical Society, Pennington, NJ, 1984, p. 527.
43. K. Aoki and M. Sakai, *J. Electroanal. Chem. 267* (1989) 47.
44. B. Noble, *Methods Based on the Wiener-Hopf Techniques for the Solution of Partial Differential Equations*, Pergamon Press, London, 1958.
45. A. J. Bard and L. R. Faulkner, *Electrochemical Methods: Fundamentals and Applications*, John Wiley & Sons, New York, 1980, pp. 290–292.
46. K. Tokuda and H. Matsuda, *J. Electroanal. Chem. 52* (1974) 421.
47. H. Matsuda, *J. Electroanal. Chem. 16* (1968) 153.
48. K. Aoki, K. Tokuda, and H. Matsuda, *J. Electroanal. Chem. 235* (1987) 87; 4π in Equation 30 should be replaced by $4/\pi$.
49. A. M. Bond, K. B. Oldham, and C. G. Zoski, *J. Electroanal. Chem. 245* (1988) 71.
50. M. Fleischmann, J. Daschbach, and S. Pons, *J. Electroanal. Chem. 263* (1989) 189.
51. D. R. Barker and M. W. Verbrugge, *J. Electrochem. Soc. 137* (1990) 205.
52. *Handbook of Mathematical Functions*, M. Abramowitz and I. A. Stegun, Eds., Dover Publications, New York, 1970, pp. 589–598.
53. K. B. Oldham and C. G. Zoski, *J. Electroanal. Chem. 313* (1991) 17.
54. T. Abe, K. Itaya, I. Uchida, K. Aoki, and K. Tokuda, *Bull. Chem. Soc. Jpn. 61* (1988) 3417.
55. J. Osteryoung, *Electroanalytical Chemistry, Vol. 14, Square-Wave Voltammetry*, Marcel Dekker Inc., New York, 1989.
56. C. Amatore, B. Fosset, J. Bartelt, M. R. Deakin, and R. M. Wightman, *J. Electroanal. Chem. 256* (1988) 255.
57. D. R. Baker, M. W. Verbrugge, and J. Newman, *J. Electroanal. Chem. 314* (1991) 23.
58. A. Rius, S. Polo and J. Llopis, *An. Fis. Quim. 45B* (1949) 1029.
59. K. Aoki, K. Honda, K. Tokuda, and H. Matsuda, *J. Electroanal. Chem. 182* (1985) 267.
60. K. Aoki, H. Kaneko, and K. Nozaki, *J. Electroanal. Chem. 247* (1988) 29.

61. K. Aoki, K. Tokuda, and H. Matsuda, *J. Electroanal. Chem. 206* (1986) 47.
62. K. Aoki and H. Kaneko, *J. Electroanal. Chem. 247* (1988) 17.
63. K. Aoki, M. Ishida, and K. Tokuda, *J. Electroanal. Chem. 245* (1988) 39.
64. S. Sujaritvanichpong, K. Aoki, K. Tokuda, and H. Matsuda, *J. Electroanal. Chem. 199* (1986) 271.
65. K. Aoki, K. Tokuda, and H. Matsuda, *Denki Kagaku 54* (1986) 1010.
66. A. Szabo, D. K. Cope, D. E. Tallman, P. M. Kovach, and W. Wightman, *J. Electroanal. Chem. 217* (1987) 417.
67. K. Aoki, K. Tokuda, and H. Matsuda, *J. Electroanal. Chem. 230* (1987) 61.
68. S. Coen, D. K. Cope, and D. E. Tallman, *J. Electroanal. Chem. 215* (1986) 29.
69. D. K. Cope, C. H. Scott, U. Kalapathy, and D. E. Tallman, *J. Electroanal. Chem. 280* (1990) 27.
70. K. Aoki and K. Tokuda, *J. Electroanal. Chem. 237* (1987) 163.
71. T. Gueshi, K. Tokuda, and H. Matsuda, *J. Electroanal. Chem. 101* (1979) 29.
72. T. Gueshi, K. Tokuda, and H. Matsuda, *J. Electroanal. Chem. 102* (1979) 41.
73. H. Reller, E. Kirowa-Eisner, and E. Gileadi, *J. Electroanal. Chem. 138* (1982) 65.
74. D. Shoup and A. Szabo, *J. Electroanal. Chem. 160* (1984) 19.
75. H. S. White, H. S. Kittlesen, and M. S. Wrighton, *J. Am. Chem. Soc. 106* (1984) 5375.
76. D. Bélanger and M. S. Wrighton, *Anal. Chem. 59* (1987) 1426.
77. W. Thormann, P. van den Bosch, and A. B. Bond, *Anal. Chem. 57* (1985) 2764.
78. C. E. Chidsey, B. J. Feldman, C. Lundgren, and R. W. Murray, *Anal. Chem. 58* (1986) 601.
79. D. G. Sanderson and L. B. Anderson, *Anal. Chem. 57* (1985) 2388.
80. *Handbook of Mathematical Functions*, M. Abramowitz and I. A. Stegun, Eds., Dover Publications, New York, 1970, p. 569.
81. O. Niwa, M. Morita, and H. Tabei, *J. Electroanal. Chem. 267* (1989) 291.
82. K. Aoki, *J. Electroanal. Chem. 270* (1989) 35.
83. K. Aoki, *Electroanalysis 2* (1990) 229.
84. A. Szabo, *J. Phys. Chem. 91* (1987) 3108.
85. M. Fleischmann and S. Pons, *J. Electroanal. Chem. 222* (1987) 107.
86. D. K. Cope, C. H. Scott, and D. E. Tallman, *J. Electroanal. Chem. 285* (1990) 49.
87. A. M. Bond, D. Luscombe, K. B. Oldham, and C. G. Zoski, *J. Electroanal. Chem. 249* (1988) 1.
88. Z. Szakály, L. Dazuházi, and G. Farsang, *J. Electroanal. Chem. 305* (1991) 185.
89. K. Aoki, K. Tokuda, and H. Matsuda, *J. Electroanal. Chem. 146* (1983) 417.
90. K. Aoki, K. Tokuda, and H. Matsuda, *J. Electroanal. Chem. 160* (1984) 33.